The Astrophysical Journal Letters, 932:L25 (10pp), 2022 June 20 https://doi.org/10.3847/2041-8213/ac756f

GB6 J2113+1121: A Multiwavelength Flaring γ-Ray Blazar Temporally and Spatially Coincident with the Neutrino Event IceCube-191001A

Neng-Hui Liao[1], Zhen-Feng Sheng[2,6], Ning Jiang[2,6], Yu-Ling Chang[3], Yi-Bo Wang[2,6], Dong-Lian Xu[3], Xin-Wen Shu[4], Yi-Zhong Fan[5], and Ting-Gui Wang[2,6]

[1] Department of Physics and Astronomy, College of Physics, Guizhou University, Guiyang 550025, People's Republic of China; nhliao@gzu.edu.cn
[2] Key Laboratory for Research in Galaxies and Cosmology, Department of Astronomy, The University of Science and Technology of China, Chinese Academy of Sciences, Hefei, Anhui 230026, People's Republic of China; twang@ustc.edu.cn
[3] Tsung-Dao Lee Institute, Shanghai Jiao Tong University, Shanghai 200240, People's Republic of China
[4] Department of Physics, Anhui Normal University, Wuhu, Anhui, 241000, People's Republic of China
[5] Key Laboratory of Dark Matter and Space Astronomy, Purple Mountain Observatory, Chinese Academy of Sciences, Nanjing 210034, People's Republic of China
[6] School of Astronomy and Space Science, University of Science and Technology of China, Hefei, Anhui 230026, People's Republic of China
Received 2022 February 8; revised 2022 May 8; accepted 2022 June 2; published 2022 June 21

Abstract

A radio-emitting tidal disruption event (AT2019dsg) is proposed as a likely counterpart to the IceCube neutrino event IC 191001A. In this work, we have revisited the Fermi-LAT data in the direction of the neutrino and confirmed no signal at the site of AT2019dsg. Instead, at the edge of the 90% confidence level error region of this neutrino, there is a γ-ray transient source associated with the blazar GB6 J2113+1121. In 2019 May, GB6 J2113 +1121 was undergoing a γ-ray flare that is unprecedented since the start of the Fermi-LAT operation, with a variability amplitude of about 20 fold. Similar violent flares of GB6 J2113+1121, unobserved before, have also been detected in the optical bands. Moreover, the blazar remained in a high-flux state in the infrared bands when IC 191001A arrived, though the blazar 's γ-ray and optical activities have temporarily ceased. Motivated by this spatial and temporal coincidence, we suggest that GB6 J2113+1121 is a candidate to be the counterpart to IC 191001A. The jet properties of GB6 J2113+1121 are investigated, which are found to be comparable with that of neutrino-emitting blazars (candidates). A specific analysis of archival IceCube data in this direction and future observations would put further constraints on the origin of the neutrino.

Unified Astronomy Thesaurus concepts: Galaxy jets (601); Radio loud quasars (1349); Gamma-ray sources (633)

1. Introduction

The IceCube Neutrino Observatory (Aartsen et al. 2017b) at the south pole[7] has detected high-energy neutrinos of astrophysical origin (IceCube Collaboration 2013), opening a new window into the nonthermal universe. Unlike charged cosmic rays (CRs) that could be affected by ambient matter and radiation fields as well as the deflection due to magnetic fields during propagation or γ-ray photons that might suffer significant attenuation, neutrinos travel undisturbed, allowing us to directly probe a large number of extreme cosmic environments that are otherwise opaque (Aartsen et al. 2018). The arrival directions of the IceCube neutrinos are isotropically distributed, which indicates a predominantly extragalactic origin. Extragalactic cosmic accelerators, for instance, active galactic nucleus (AGN) jets (e.g., Böttcher et al. 2013; Becker Tjus et al. 2014), γ-ray bursts (e.g., Waxman 1995), starburst galaxies (e.g., Loeb & Waxman 2006), as well as galaxy clusters (e.g., Murase et al. 2008), are hence reasonable neutrino contributors (for a review, see Ahlers & Halzen 2015). However, no compelling evidence for significant clusters of IceCube neutrinos in either space or time has been found (Aartsen et al. 2015, 2017a, 2020; IceCube Collaboration et al. 2021). Interestingly, a 2.9σ significance excess against the background is found 0°.35 from the Seyfert II galaxy NGC 1068 by targeting a predefined list of 110 sources (Aartsen et al. 2020). Therefore, a substantial fraction of the observed diffuse neutrinos is suggested to be from the contribution of weak sources that are individually below the point-source sensitivity (Murase & Waxman 2016). On the other hand, neutrino transients have been proposed to be detectable (e.g., Halzen & Kheirandish 2016).

A notable case is the IceCube detection of a 0.3 PeV muon neutrino (IC-170922A) from the position-compatible blazar TXS 0506+056 coinciding with a multiband flaring period at 3σ significance (IceCube Collaboration et al. 2018a). A 160 day-long neutrino flare (3.5σ significance) has also been found in that direction, though no accompanying electromagnetic activities of the blazar were exhibited (IceCube Collaboration et al. 2018b). Blazars, including flat-spectrum radio quasars (FSRQs) and BL Lacertae objects (BL Lacs), are an extreme subclass of AGNs whose strong relativistic jets are well aligned with our line of sight (Blandford & Rees 1978; Blandford et al. 2019). The highly beamed jet emissions are overwhelming and hence the emission of blazars is highly variable (Wagner & Witzel 1995; Ulrich et al. 1997). The universal spectral energy distributions (SEDs) of blazars feature a two-bump shape in the log $\nu F\nu$–log ν plot, where one is from synchrotron emission while the other one extends to the γ-ray domain. In the hadronic radiation scenarios, γ-ray emissions of blazars could be from the decay of neutral pions generated by the interaction between cosmic-ray (CR) nuclei and ambient matter or radiation fields; meanwhile, charged pions are produced at the same time, leading to the generation of neutrinos (Stecker et al. 1991; Mannheim 1993; Atoyan & Dermer 2001).

[7] https://icecube.wisc.edu/

Therefore, the observed γ-ray emissions and neutrinos are thought to be tightly connected. Furthermore, in addition to these two messengers, hadronic cascades also produce electromagnetic emissions at lower energies, and hence multiwavelength observations play a key role in identifying neutrino emitters (e.g., Murase et al. 2018; Garrappa et al. 2019b; Franckowiak et al. 2020; Giommi et al. 2020). Because neutrinos are solely produced by hadronic processes but γ-ray photons can also be from leptonic processes (i.e., inverse Compton scattering of soft photons; Maraschi et al. 1992; Dermer & Schlickeiser 1993; Sikora et al. 1994; Błażejowski et al. 2000), detections of neutrinos from blazars provide a unique insight into AGN jets (Ansoldi et al. 2018).

On 2019 October 1 at 20:09:18.17 UT, IceCube detected a track-like ~0.2 PeV neutrino event (IC 191001A) with a probability of 58.9% (i.e., `Gold` alert streams) of being of astrophysical origin, with an arrival direction of R.A. $314.08^{+6.56}_{-2.26}$° and decl. $12.94^{+1.50}_{-1.47}$° (IceCube Collaboration 2019). Within such a region, there are two known γ-ray sources categorized in the fourth Fermi γ-ray source catalog (4FGL; Abdollahi et al. 2020) (Garrappa et al. 2019a). In addition, a spatially coincident radio-emitting tidal disruption event (TDE), AT2019dsg, was discovered about 175 days earlier than the detection of IC 191001A (Stein et al. 2019). After investigations of the multiwavelength variability properties of the TDE, it was proposed to be a likely association for the neutrino, especially considering the continuously increasing radio emission (Stein et al. 2021). Analyzing roughly 1 yr-long Fermi-LAT data around the arrival time of IC 191001A, no significant γ-ray emissions of the two 4FGL sources are detected. Anyhow, a new γ-ray source (labeled as Fermi J2113.8+1120 toward the flat spectral source GB6 J2113+1121) emerged at the edge of the 90% confidence level (C. L.) localization error box of the neutrino (Stein et al. 2021); also see Figure 1. A similar temporal investigation of Fermi J2113.8+1120 also yielded no clear flux enhancement at the exact arrival time (i.e., within 1 month) of the neutrino, and hence this source was also suggested to be unlikely related to the neutrino (Stein et al. 2021).

In this Letter, we carry out thorough investigations of the multiwavelength properties of GB6 J2113+1121 based on 12.6 yr Fermi-LAT data from the start of its operation as well as archival data from Swift, Zwicky Transient Facility (ZTF), and WISE, along with an optical spectroscopic observation carried out by the Hale 5 m telescope (Section 2). Discussions of its broadband variability behaviors and the potential to be a neutrino counterpart are given in Section 3. We adopt a ΛCDM cosmology with $\Omega_M = 0.32$, $\Omega_\Lambda = 0.68$, and a Hubble constant of $H_0 = 67\ \mathrm{km^{-1}\ s^{-1}\ Mpc^{-1}}$ (Planck Collaboration et al. 2014).

2. Data Analysis and Results

GB6 J2113+1121 is known as a flat spectral radio source (Bennett et al. 1986; Myers et al. 2003; Koay et al. 2011), with a spectroscopic redshift measurement of 1.316 (Pursimo et al. 2013). Based on the SDSS g-band magnitude (Adelman-McCarthy et al. 2007) and the NVSS 1.4 GHz flux density (Condon et al. 1998), the radio loudness is estimated to be as high as ≃3000.

2.1. Fermi-LAT Data

The first 12.6 yr (MJD 54,683−59,309) `SOURCE` type (`evclass`=128 and `evtype`=3) Fermi-LAT `Pass 8` data with energy range between 0.1 and 500 GeV are collected. The analysis is carried out with the `Fermitools` software version `2.0.8` and the accompanying `Fermitools-data` version `0.18`. The zenith angle cut (i.e., <90°) and the recommended quality-filter cuts (i.e., `DATA_QUAL==1 && LAT_CONFIG==1`) are adopted to filter the entire photon data. `Unbinned` likelihood analyses implemented in the `gtlike` task are used to extract γ-ray flux and spectrum. The significance level of detecting a γ-ray source is quantified by the test statistic ($\mathrm{TS} = -2\ln(L_0/L)$, Mattox et al. 1996), where L and L_0 are the maximum likelihood values for the model with and without the target source, respectively. During the likelihood analysis, 4FGL sources within 15° of the radio position of GB6 J2113+1121, as well as the diffuse γ-ray emission templates (i.e., `gll_iem_v07.fits` and `iso_P8R3_SOURCE_V3_v1.txt`), are embraced. Parameters of the background sources within the 10° region of interest (ROI) centered at the target location as well as normalizations of the two diffuse templates are left free, whereas others are frozen as the 4FGL values. If new γ-ray sources (i.e., TS > 25) are found from the residual TS maps, the initial background model is updated and the likelihood fitting is then reperformed. In the temporal analysis, weak background sources (i.e., TS < 10) are removed from the analysis model. For sources with TS < 10, the `pyLikelihood UpperLimits` tool is adopted to calculate the 95% C. L. upper limit instead of a flux estimation.

The analysis of the entire data set suggests the existence of a significant γ-ray source (TS = 217.4) toward GB6 J2113+1121, along with three other γ-ray sources (TS ⩽ 50, not in 4FGL-DR2[8]) at the edge of the ROI, among which one may associate with CGRaBS J2051+1743 (Healey et al. 2008). The optimized location of the central γ-ray source is at R.A. 318.°4855, decl. 11.°3261 with a 95% C. L. error radius of 4.′3. Considering that the separation between the γ-ray location and radio position of GB6 J2113+1121 is 1.′9, and no other known radio source is found within the error radius, GB6 J2113+1121 is probably the low-energy counterpart of the γ-ray source. Assuming the single power-law spectral distribution (i.e., $dN/dE \propto E^{-\Gamma}$, where Γ is the photon index), the averaged γ-ray flux is given, $(1.30 \pm 0.15) \times 10^{-8}\ \mathrm{ph\ cm^{-2}\ s^{-1}}$, as well as a relatively soft spectrum (i.e., $\Gamma_\gamma = 2.58 \pm 0.07$).

A six-month time bin γ-ray light curve for GB6 J2113+1121 is extracted; see Figure 1. It is confirmed that the target has remained at a quiescent flux state since the beginning of the Fermi-LAT operation for over 10 yr, but then a strong γ-ray flare comes out. Besides the target, the temporal behaviors of the background sources are also examined; no similar behaviors to that of the target are found. Therefore, the variability of the target is suggested to be intrinsic rather than artificially caused by the background sources. Light curves of the two 4FGL sources (i.e., 4FGL J2052.7+1218 and 4FGL 2115.2+1218) that fall into the neutrino localization error box are also extracted, from which no significant (<3σ, Nolan et al. 2012) variability is found. Moreover, it is confirmed that they are not detected by Fermi-LAT (i.e., TS < 20) by selecting 1 yr data centered at the arrival time of the neutrino (Stein et al. 2021). Therefore, they are not preferred to be the neutrino counterpart. We divide the time range of the entire data set into two separate parts at MJD 58,383, corresponding to different flux states of GB6 J2113+1121. The target is barely detected by Fermi-LAT (TS = 24.7) in the previous period, with a flux estimation of $(4.7 \pm 1.1) \times 10^{-9}\ \mathrm{ph\ cm^{-2}\ s^{-1}}$. On the other hand, analyses of

[8] https://fermi.gsfc.nasa.gov/ssc/data/access/lat/10yr_catalog/

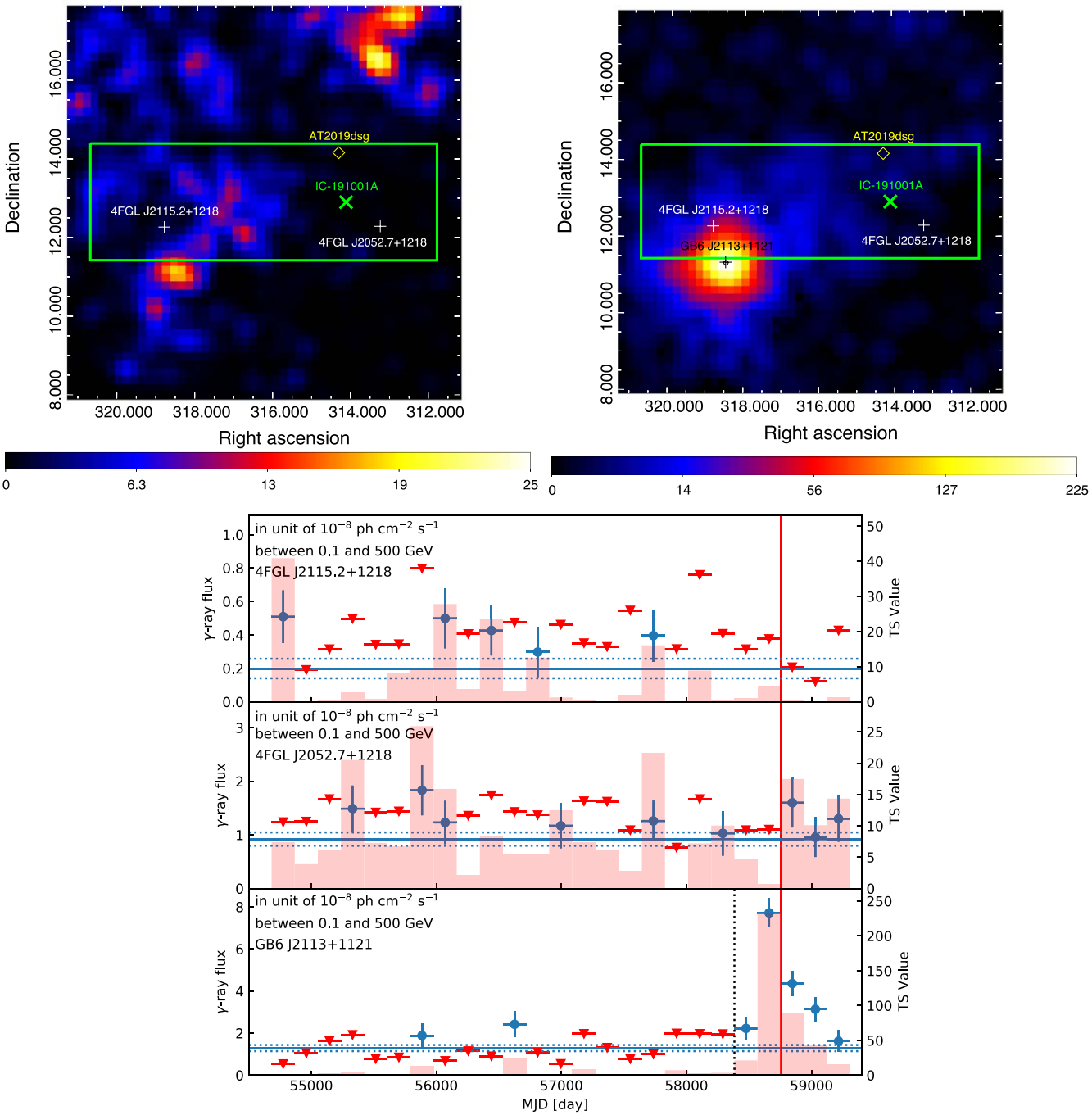

Figure 1. Upper panels: smoothed γ-ray test static (TS) maps ($10^\circ \times 10^\circ$ scale with $0.^\circ2$ per pixel; GB6 J2113+1121 not included in the mode file) of the region that is spatially compatible with the arrival direction of the neutrino IC 191001A. The left one is based on the Fermi-LAT data with a time range between MJD 54,683 (i.e., the beginning of its operation) and MJD 58,383 (marked as a black vertical dashed line in the bottom panel), while the right one corresponds to the rest of the Fermi-LAT data. The black circle represents the 95% C. L. γ-ray localization error radius of GB6 J2113+1121, and the black cross corresponds to its radio location. Bottom panel: half-year time bin γ-ray light curves of the three γ-ray sources spatially coincident with the neutrino IC 191001A. Blue circles and red triangles are flux estimations and upper limits, and TS values corresponding to each time bin are also shown. The horizontal lines represent the averaged fluxes of the sources for the entire data set along with the 1σ uncertainties. The red vertical line marks the arrival time of the neutrino IC 191001A.

the last period reveal a significant γ-ray source (TS = 327.6) with flux reaching $(3.2 \pm 0.3) \times 10^{-8}$ ph cm^{-2} s^{-1}, roughly seven times the value in the quiescent flux state. A follow-up localization analysis confirms that GB6 J2113+1121 remains within the γ-ray location error radius; also see Figure 1. To further investigate the γ-ray variability properties, a monthly light curve focusing on the data in the high-flux state is extracted; see Figure 2. The target is detectable for nearly 1 yr. A month prior, the light curve begins with a rapid flux ascent wherein the target turns brighter with a peak flux of $(1.1 \pm 0.2) \times 10^{-7}$ ph cm^{-2} s^{-1} while the background emission is dominant. The decline phase is longer than the ascending phase, and it disappears around MJD 58,750. Interestingly, a mild second flare where the flux remains at $\sim 4 \times 10^{-8}$ ph cm^{-2} s^{-1} follows, then the target is back to the quiescent state a few months later. Spectral analysis of this one-year period suggests a probable spectral hardness (i.e., $\Gamma_\gamma = 2.37 \pm 0.07$) compared with that obtained from the entire data set. A sophisticated spectral template rather than a single

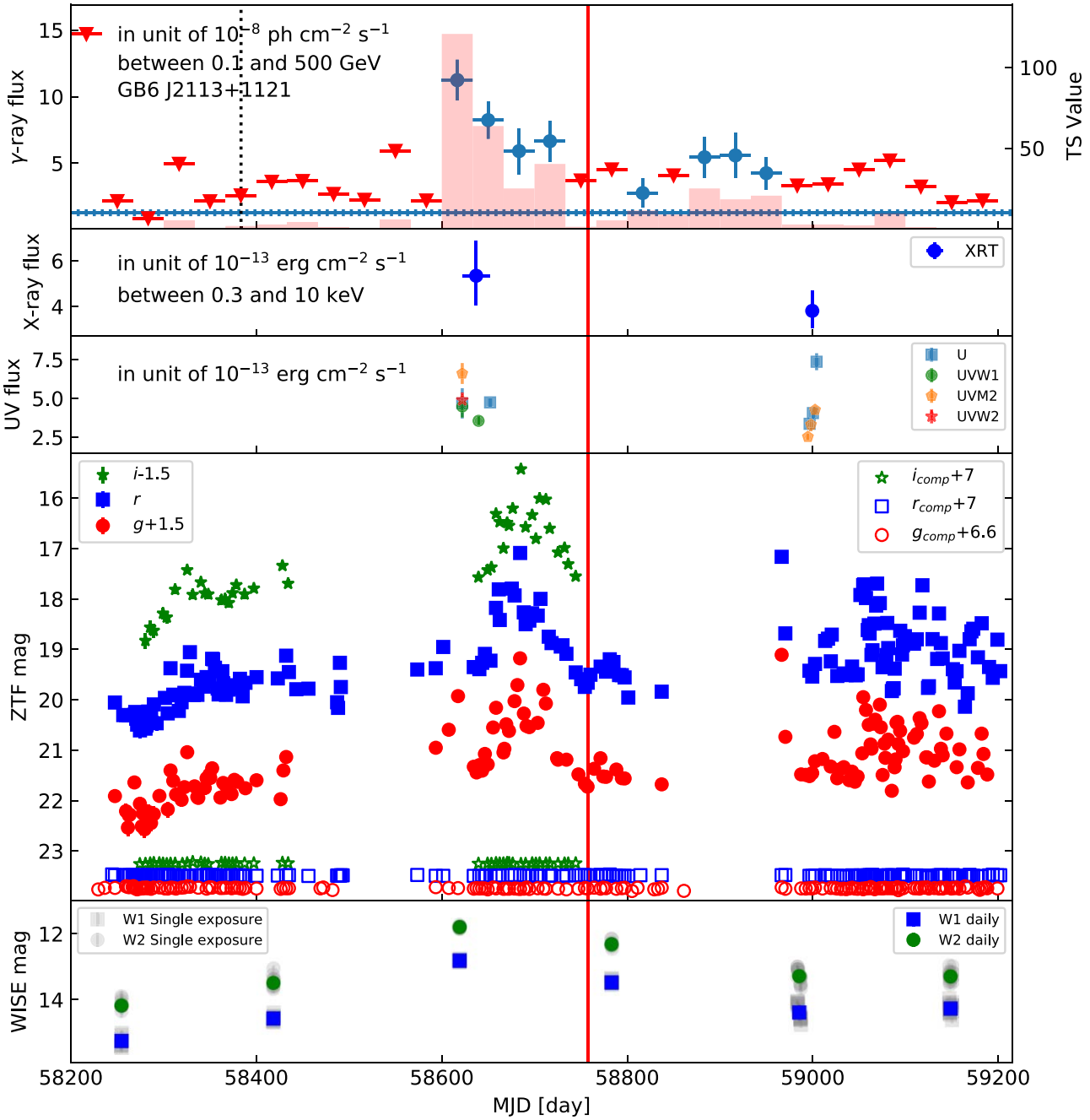

Figure 2. Multiwavelength light curves of GB6 J2113+1121. In the monthly γ-ray light-curve panel, the horizontal and black dashed vertical lines are the same as those in Figure 1. For the Swift-UVOT measurements, corrections of the Galactic absorption have been carried out (Cardelli et al. 1989; Schlafly & Finkbeiner 2011). For the ZTF light curves, the solid markers represent the magnitudes of the target, while the hollow ones correspond to average values of the comparison stars in the same field. The red vertical line across all panels marks the arrival time of the neutrino.

power-law function is adopted; no significant spectral curvature is found. The energy of the most energetic γ-ray photons received from GB6 J2113+1121 then is about 8 GeV. A 10 day time bin light curve focusing on the rapid ascending phase is also extracted and the peak time of the first flare is around MJD 58,615; however, no evidence of intraday variability is found.

2.2. Swift Data

There are in total nine visits from the Neil Gehrels Swift Observatory (Gehrels et al. 2004) to GB6 J2113+1121. FTOOLS software version 6.28 is adopted to analyze the XRT photon-counting mode data and the UVOT images. For the XRT data, the initial event cleaning `xrtpipeline` procedure with standard quality cuts is carried out. The `xselect` task is used to extract the source spectra from a circular region with a radius of 12 pixels while the background spectra are from a larger circle (i.e., 50 pixels) in a blank area. Then, the ancillary response files are created by the response matrix files taken from the calibration database with `xrtmkarf` to facilitate the subsequent spectral analysis. We group the spectra to have at least one count per bin using the `cstat` approach. Setting the absorption column density as the Galactic

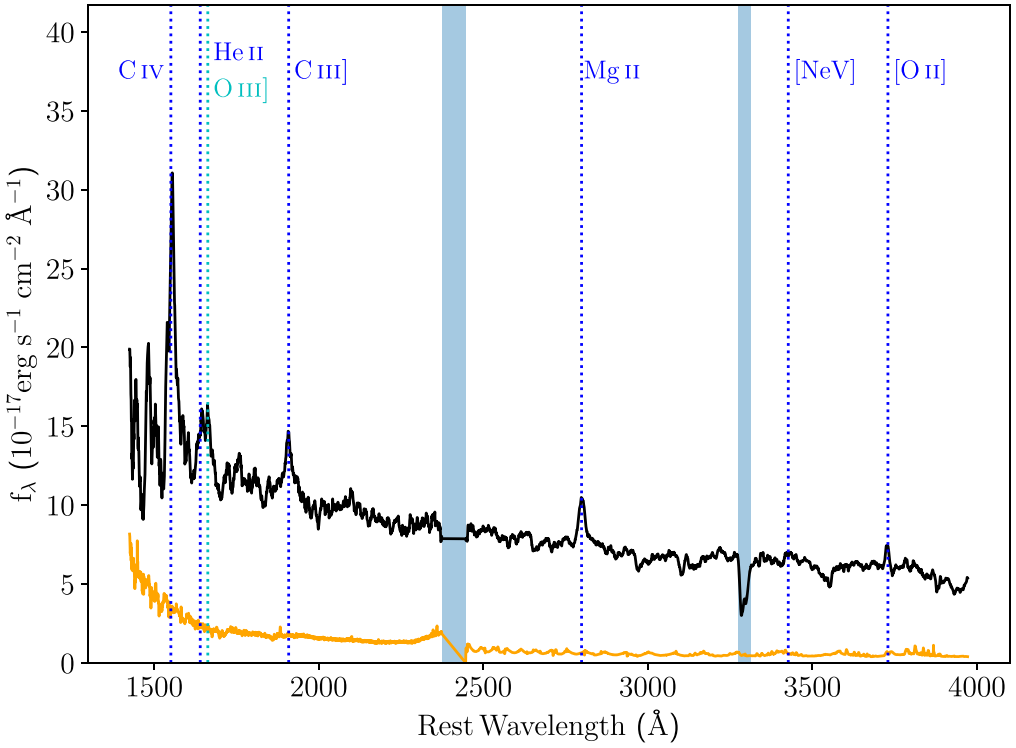

Figure 3. P200 spectrum. The spectrum is plotted in black and smoothed by a window with a length of 16 Å, while the uncertainty is in orange. The vertical dotted lines mark the main emission lines. The blue shaded regions represent the position of the dichroic or the uncorrected telluric.

value (i.e., $5.8 \times 10^{20}\,\mathrm{cm}^{-2}$), an analysis of the entire data set (totally 107 net photons) gives an averaged unabsorbed 0.3–10.0 keV flux of $4.3^{+1.3}_{-0.9} \times 10^{-13}$ erg cm^{-2} s^{-1} ($\mathcal{C}$-statistic/d.o.f, 146/105; Cash 1979). Meanwhile, a hard spectrum is suggested (i.e., $\Gamma_x \sim 1.3$). X-ray temporal properties are investigated; however, no significant variability can be found due to the limited statistics. For the UVOT images, the magnitudes are extracted by the aperture photometry (i.e., the `uvotsource` task), with a 5″ circular aperture for the target along with a background one in a larger source-free region. Significant variability is revealed in the UV emission densities of the target. For instance, a flux rise of 0.85 mag in the *U* band is detected between observations at MJD 58,996.6 and 59004.2.

2.3. Optical Data

2.3.1. Optical Spectrum

The spectrum is taken from the Double Spectrograph (the dichroic D55) on the Hale 200 inch telescope at the Palomar Observatory on MJD 59,383. The exposure is split into four 450 s periods through a 2.″0 slit. The data are reduced by `Pypeit`[9] (Prochaska et al. 2020). The resolving power is $R \sim 720$ and the median signal to noise is 9.6. After dereddening the Milky Way extinction (Schlegel et al. 1998), the best-fitting continuum model is $f = 8.27 \times (\lambda/3000)^{-1.04}$. Several emission lines are distinct, marked in Figure 3, from which the redshift estimation of 1.316 ± 0.002 is given, confirming the result in Pursimo et al. (2013). We get $\log \lambda L_\lambda(3000\,\text{Å}) = (24.16 \pm 0.04) \times 10^{44}$erg s^{-1}, and the flux and FWHM of Mg II are $(9.8 \pm 1.68) \times 10^{-16}$erg cm^{-2} s^{-1} and (2714 ± 597) km s^{-1}, respectively. Using the empirical virial BH mass relation provided by Shen et al. (2008), we get $\log(M_{\rm BH}/M_\odot) \gtrsim 8.2$, in the case of a disk-like geometry of the broad-line region (BLR). Adopting the bolometric luminosity correction $L_{\rm bol} \sim (5.18 \pm 0.19) L_{3000}$ (Runnoe et al. 2012), which is likely overestimated due to the jet contribution, we can infer the Eddington ratio $L_{\rm bol}/L_{\rm edd} \lesssim 0.6$.

2.3.2. ZTF Light-curve Data

The ZTF (Graham et al. 2019; Bellm et al. 2019; Masci et al. 2019; PTF Team 2020) data from its Public Data Release 6[10] are collected. Initially, the coadded reference images are examined, from which GB6 J2113+1121 is distinguishable in the *g*, *r*, and *i* bands. Light curves in these three bands are extracted for objects falling within a 5″ radius from a position of the target. Only frames satisfying `catflags=0` and `chi<4` are selected.[11] There are in total 149, 201, and 40 exposures in the *g*, *r*, and *i* bands, respectively, covering the time range between MJD 58,200 and MJD 59,200; see Figure 2. Magnitudes of five comparison stars (∼17 mag) from the PTF Photometric Calibrator Catalog (Ofek et al. 2012) lying 10′ from the target are also derived, for which the standard deviations are less than 0.05 mag; also see Figure 2. The significant optical variability of GB6 J2113+1121 is revealed by the ZTF light curves, from which a remarkable signature is a violent flare peaking at MJD 58,684 captured in all three bands. Considering that the target is barely detected in a single exposure at the beginning of the ZTF operation, the brightening for the flare reaches over 3.0 mag. It is interesting that there is another major flare as violent as the former one that might peak

[9] https://pypeit.readthedocs.io/en/latest/

[10] https://www.ztf.caltech.edu/page/dr6

[11] http://web.ipac.caltech.edu/staff/fmasci/ztf/extended_cautionary_notes.pdf

around MJD 58,966, though only its descent phase is caught. Because the first flare is well sampled, it is worthy of attention. It took 44 days for the flux densities of the target to reach the peak values ($g_{\rm peak} = 17.68 \pm 0.02$, $r_{\rm peak} = 17.08 \pm 0.02$, and $i_{\rm peak} = 16.92 \pm 0.02$ mag) from MJD 58,640 ($g = 19.80 \pm 0.09$, $r = 19.39 \pm 0.07$, and $i = 19.07 \pm 0.07$ mag). The flux descent phase begins with a rapid flux density decay (i.e., a faintness of $\simeq$1.1 mag within 4 days in the g and r bands). Then a slow decay lasting for about 2 months followed ($g = 20.17 \pm 0.11$ and $r = 19.74 \pm 0.09$ mag at MJD 58,754). Between the two major flares, no significant activities are detected and the source stays in a low state ($g \sim$20.0 and $r \sim$19.5 mag). Based on the limited data, the descent phase of the second flare only lasts about 20 days, from MJD 58,966 ($g_{\rm peak} = 17.61 \pm 0.02$ mag) to MJD 58,987 ($g = 19.98 \pm 0.10$ mag). Interestingly, because the g-band magnitude at MJD 58,970 is 19.23 ± 0.06 mag, a rapid flux density decay (i.e., a dimming of 1.6 mag within 4 days) is detected. Since then, optical emissions of GB6 J2113+1121 in 2020 are still active; however, no flares as violent as the major flares have been detected.

2.4. WISE Data

We retrieve single-exposure photometric data in the W1 and W2 bands (centered at 3.4 and 4.6 μm in the rest frame) from the Wide-field Infrared Survey Explorer (WISE; Wright et al. 2010; WISE Team 2019) and the Near-Earth Object WISE Reactivation mission (NEOWISE-R; Mainzer et al. 2014; WISE Team 2020). Following our previous work (Sheng et al. 2017, 2020), we filter the bad data points with poor image quality ("qi_fact" < 1), a small separation from the South Atlantic Anomaly ("SAA"<5), and the flagged moon masking ("moon mask" = 1). First, we bin the data in each epoch (nearly half-year) using the median value to probe the long-term variability of the target, while the sample standard deviation value is taken to be the conservative estimate of the uncertainty. A violent long-timescale variability is clearly exhibited in the WISE light curves; see Figure 2. For instance, comparing the observations at MJD 58,255 and 58,619, a brightening of 2.4 mag in both W1 and W2 bands is detected. In fact, the variability amplitude can be larger considering that the target is dim at the beginning of WISE operation (i.e., $W1 = 16.2 \pm 0.3$ mag, $W2 = 14.9 \pm 0.2$ mag at MJD 55,332). On the other hand, rapid IR variability with amplitudes of about 0.5 mag within 0.5 days (W1) and 0.3 days (W2) at MJD 59,146 is observed. The variability of the IR color is also checked, and no such evidence is found.

2.5. Implications of the Multiwavelength Properties of GB6 J2113+1121

Here, a thorough investigation of the multiwavelength behaviors of the flat spectral radio source GB6 J2113+1121 has been performed. The most distinct feature is the emergence of a giant flare in long-term IR, optical, and γ-ray light curves. The flare brings large variability amplitudes, roughly a 25 fold flux increase in the IR and γ-ray regimes and 17 fold in optical bands. The violent variability can be naturally explained as an activity induced by the AGN jet (e.g., Madejski & Sikora 2016; Blandford et al. 2019). The peak times (around MJD 58,600) of the giant flare at different wavelengths are consistent, though the data sampling of the WISE light curves is sparse. Meanwhile, no activity that is as violent as the giant flare is found from the first 10 yr of monitoring by Fermi-LAT as well as observations of WISE and iPTF then. The similar shapes of the multiwavelength light curves provide decisive evidence supporting the association between the γ-ray source and the low-energy counterpart; hence, GB6 J2113+1121 is a γ-ray-emitting FSRQ.

In addition to the long-term variability, rapid variations have been found in the IR and optical domains from which the doubling timescale at the source frame can be simply constrained as $\tau_{\rm doub,source} = \Delta t \times ln2/ln(F_1/F_2)/(1+z)$. Therefore, $\tau_{\rm doub,source}$ is inferred to be $\sim$19 hr for the sharp decline in the ZTF g band around MJD 58,970 and $\sim$5 hr for the dense monitoring of WISE at MJD 59,146. In the perspective of the short-variability timescale together with its strong γ-ray emission, the value of the Doppler factor δ of the emitting jet blob should be high enough to avoid severe attenuation on γ-rays from soft photons via the $\gamma\gamma$ process. The absorption opacity can be calculated as (Dondi & Ghisellini 1995)

$$\tau_{\gamma\gamma}(x') = \frac{\sigma_{\rm T}}{5} n'(x_{\rm t}') x_{\rm t}' R', \quad (1)$$

where $x' = h\nu'/m_e c^2$ is the dimensionless energy of the γ rays and $x_{\rm t}'$ for the target soft photon in the comoving frame, $n'(x_{\rm t}')$ is the comoving differential number density of the target photon per energy, $\sigma_{\rm T}$ is the scattering Thomson cross section, and R' is the absorption length. The absorbing soft photons could be from the jet itself and hence, in this case, the absorption length is equal to the radius of the emitting jet blob, $R_\gamma{}' = c\tau'_{\rm var} \lesssim \delta c \tau_{\rm doub,source}$. Because the most energetic γ-ray photon is at $\simeq$ 8GeV, adopting the soft radiation ($\sim 5 \times 10^{45}$ erg s^{-1} at several keV) from the Swift-XRT observation and $t_{\rm IR,source}$ of $\sim$5 hr, a constraint of $\delta \gtrsim 5$ can be obtained. On the other hand, because significant spectral features are revealed by the P200 spectrum, the soft photons could be external to the jet (e.g., from the accretion disk or broad emission lines), depending on the location of the jet dissipation region. Assuming a conical jet geometry (i.e., $\Gamma\theta = 1$, where Γ is the jet bulk Lorentz factor and θ is the jet-opening angle), the location can be determined as $r_\gamma = \delta R_\gamma{}' \sim 0.05$ pc, for which a typical Doppler factor value of 15 (e.g., Liodakis et al. 2017) is used. Compared with the typical radius of the BLR (i.e., $\sim$0.1 pc; Tavecchio et al. 2010), the emitting jet blob is likely embedded in the radiation of the broad emission lines. However, due to insufficient information on the broad emission lines in the UV band (Liu & Bai 2006; Poutanen & Stern 2010), constraints from the external absorption on the γ rays cannot be achieved.

The multiwavelength data allow us to draw broadband SEDs of GB6 J2113+1121. As shown in Figure 4, typical two-bump-shape SEDs are pictured. Though the ascending parts of the SED bumps are not well sampled, the ratio of the peak luminosities between the high-energy bump and the low-energy one is likely $\gtrsim$1, which is common for FSRQs (e.g., Finke 2013). Meanwhile, the peak frequency of the synchrotron bump is constrained to be $\lesssim 10^{14}$ Hz, and hence it is classified as a low-synchrotron-peaked source (LSP; Padovani & Giommi 1995; Abdo et al. 2010). Comparing SEDs between different flux states, the remarkable feature is violent variations in the IR, optical, and γ-ray domains. The IR domain is close to the peak frequency of the synchrotron bump and a significant dilution of the big blue bump is avoided there. In the optical

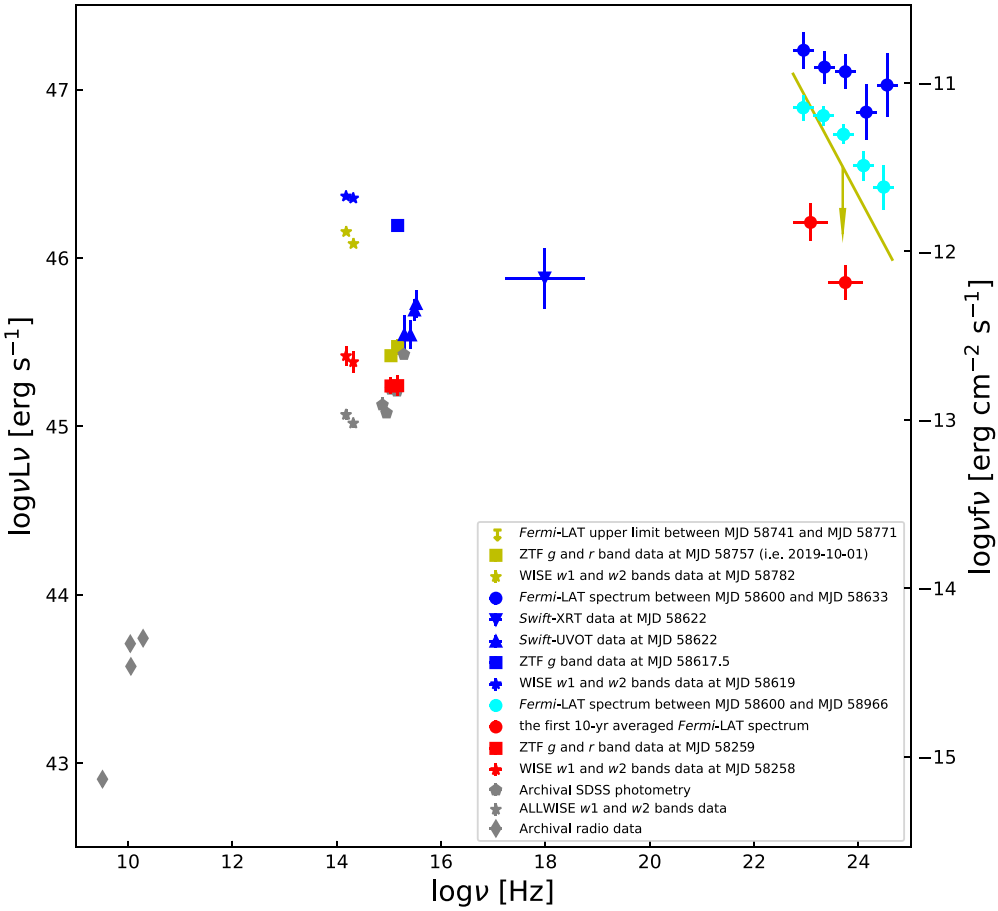

Figure 4. The broadband SED of GB6 J2113+1121. Simultaneous data are colored. The blue ones represent the high-flux state and the red ones correspond to the low-flux state. The 1 yr averaged γ-ray spectrum corresponding to the long-term high-flux state is plotted in cyan symbols. Multiwavelength data of GB6 J2113+1121 that are strictly simultaneous with the neutrino arrival are also plotted (in yellow). Nonsimultaneous data are in gray.

band, emission of the accretion disk is dominant at a low-flux state; however, the jet emission is overwhelming at a high-flux state. Interestingly, a drop in the jet emission follows and the Swift-UVOT data in the high-flux state SED is well consistent with the extrapolation of archival SDSS data and ZTF measurements at the quiescent state. For the high-energy bump peaking in the γ-ray domain, the variability amplitude is comparable with the low-energy one. SED peaks of blazars usually move to shorter wavelengths when it becomes brighter (e.g., Ghisellini et al. 2013); future simultaneous submillimeter and hard X-ray observations are crucial for investigations on the evolution of the SED of GB6 J2113+1121 during different flux states.

3. Discussion and Summary

TDEs act as evidence that activities of the massive BHs (MBHs) lurking in the galaxy centers are triggered when an orbiting star is disrupted and captured (Rees 1988). Given that the evolutionary timescale of TDEs is as short as months, the formation of an accretion disk and the launching of a possibly accompanying jet or outflow can be witnessed in real time. Benefiting from advanced multiwavelength (messenger) observations, especially the time-domain surveys, the number of detected TDEs has significantly increased (Gezari 2021). Among these, TDEs with radio detections are of special interest because the radio emissions are tightly connected to the material ejections from the MBHs (Alexander et al. 2020). The unique case is Sw J1644+57, from which luminous X-ray (i.e., $\sim 10^{48}$ erg s^{-1}) and radio emissions (i.e., $\sim 10^{44}$ erg s^{-1}), a hard X-ray spectrum, and more importantly the rapid X-ray variability have been detected, suggesting the emergence of a well-aligned relativistic jet that is similar to blazars (Bloom et al. 2011; Burrows et al. 2011; Levan et al. 2011; Zauderer et al. 2011). In principle, off-axis jetted TDE could be also detected, for instance, IGR J12580+0134 (Lei et al. 2016) and Arp 299-B AT1 (Mattila et al. 2018), from which a hard X-ray flare and a compact core jet resolved by VLBI are found, respectively. Another well-studied radio-emitting TDE is ASASSN-14li, from which thermal X-ray emissions together with weak radio emissions are observed, and the latter is proposed to be from the wind (Alexander et al. 2016; Kara et al. 2018). It is interesting to probe the location where AT2019dsg lies by comparing it with other TDEs. The X-ray (i.e., $\sim 10^{43}$ erg s^{-1}) and radio (i.e., $\sim 10^{39}$ erg s^{-1}) emissions of AT2019dsg are mild compared with Sw J1644+57 (Stein et al. 2021). Its X-ray spectrum is well described by blackbody radiation, and no signs of rapid variability in the radio and X-ray bands are reported (Stein et al. 2021). Therefore, the radio emission of AT2019dsg is proposed to be from a subrelativistic wind, which is likely akin to ASASSN-14li (Alexander et al. 2020; Stein et al. 2021).

Jetted AGNs are widely accepted as one of the most energetic accelerators in the universe (e.g., Biteau et al. 2020), and it is not surprising that blazars are the dominant population

in the extragalactic γ-ray sky (Abdollahi et al. 2020; Ajello et al. 2020). On the other hand, powerful subrelativistic winds are commonly seen in luminous AGNs (King & Pounds 2015); however, they are not notable for generating strong γ-ray emissions (i.e., in GeV and TeV energies). Nevertheless, neutrinos are proposed to be from accretion flares in super-Eddington systems, from which the lack of detection of γ-ray emissions is due to the severe $\gamma\gamma$ absorption (van Velzen et al. 2021). Actually, evidence that incoming neutrino events are associated with flaring blazars are accumulating. Prior to the famous TXS 0506+056 case (IceCube Collaboration et al. 2018a), an arriving neutrino (i.e., HESE-35) was detected in the direction of an FSRQ PKS B1424-418 from which the ejection of a new jet blob is exhibited at the same time (Kadler et al. 2016). GB6 J1040+0617, an LSP BL Lac, has been reported to be a plausible candidate for the neutrino event IC-141209A (Garrappa et al. 2019b). Interestingly, a γ-ray high-synchrotron-peaked (HSP) BL Lac, BZB J0955+3551, is found to be spatially and temporally (i.e., an X-ray flare) coincident with the IceCube neutrino event IC-200107A (Giommi et al. 2020; Paliya et al. 2020). Considering the proximity between the energies of γ-ray photons and neutrinos, searching for neutrino[12] counterparts from the GeV blazars detected by Fermi-LAT was performed. MG3 J225517+2409 together with 1H 0323+342 stand out because of detections of simultaneous γ-ray and optical flares when the neutrinos arrive, though for the latter much stronger flares without the detection of neutrinos have been seen before (Franckowiak et al. 2020). Apparently, only PKS B1424-418 and 1H 0323+342 appear to exhibit strong emission lines among these candidates. In fact, the featureless optical spectra are not only due to the inefficient accretion but also the severe dilution of the nonthermal jet radiation. For instance, TXS 0506+056 is suggested as an "intrinsic" FSRQ because of the detection of the faint [OII] line (Padovani et al. 2019). Due to the dense radiation fields external to the jets (e.g., emissions from BLR), the absorption of γ-ray photons of LSPs, especially the LSP FSRQs, could be significant, and hence, the link between the observed γ rays here and neutrinos are complicated (Kun et al. 2021). Although external photons can act as obstacles for detecting γ rays, they can also be additional target photons for pγ interactions and possibly enhance neutrino generation (e.g., Petropoulou et al. 2017).

Let us focus on the neutrino IC 191001A. First, GB6 J2113+1121 is the only γ-ray source spatially coincident with the neutrino event. The by-chance probability of such a coincidence is calculated. Because the sensitivity of IceCube improves with increasing sky decl. (Aartsen et al. 2020), only 4FGL-DR3[13] blazars (candidates) located at decl. $> -5°$ are chosen. Meanwhile, by excluding the Galactic plane (i.e., $|b| < 10°$), we estimate the surface density of blazars to be $\sim$0.09 per square degree. Therefore, the expectation number of γ-ray blazars that spatially coincide with a neutrino event like IC 191001A is roughly 2.4; obviously, spatial coincidence alone is not sufficient. Then, a Monte Carlo simulation is carried out to take into account the γ-ray flare. The central location of IC 191001A is randomized in the sky region as mentioned, whereas the size of the localization error box remains. On the other hand, additional temporal constraints are applied when selecting corresponding blazars (candidates). Like GB6 J2113+1121, they are significantly γ-ray variable, and more importantly, exhibit a clear flux enhancement at the last bin of the public 12 yr-long light curve sampled in yearly bins. After 10^4 times of simulations, we derive the probability of a chance coincidence to be $\sim$0.03, supporting the fact that GB6 J2113+1121 is a likely neutrino emitter.

Because relativistic particles accelerated in a relativistic jet emit both neutrinos and γ-ray photons, these two outputs could be proportional. Therefore, the broadband temporal behaviors of GB6 J2113+1121 are compared with those of the incoming neutrino. Initially, an epoch of one month corresponding to the γ-ray high-flux state based on the 10 day bin light curve is identified by the Bayesian block approach (Scargle et al. 2013), which is actually the bin with the largest TS value in the monthly light curve. The flux then is one order of magnitude of that during the entire IceCube operation time (i.e., since MJD 55,470). Meanwhile, the γ-ray flux of GB6 J2113+1121 in the time range between the discovery of the TDE and arrival time of the neutrino is also extracted, $(6.3 \pm 0.8) \times 10^{-8}$ ph cm^{-2} s^{-1}, roughly half of the flux in the flaring epoch. Note that compared with the discovery time of the TDE (i.e., MJD 58,582), the onset time of the blazar γ-ray-flaring epoch (i.e., MJD 58,600) is about 18 day closer to the arrival time of IC 191001A (i.e., MJD 58,758). Interestingly, the recorded onset time of the giant optical flare is even closer (i.e., MJD 58,634). For the WISE light curves, despite the sparse sampling, the infrared emissions remain in a high state at MJD 58,782, which is within one month after the arrival time of the neutrino, although the gamma-ray and optical emissions had already decreased from its outbursts. Note that for TXS 0506+056, there is also a time lag of several months between the γ-ray flux peak and the detection of IC-170922A (Garrappa et al. 2019b). Such a time mismatch could be due to the low event rate of the neutrino detection. Nevertheless, GB6 J2113+1121 is among the few Fermi blazars that are not only spatially coincident with a detected IceCube neutrino but also with detections of quasi-simultaneous multi-wavelength flares at the arrival time of the neutrino. Based on these facts, we propose that GB6 J2113+1121 is a possible counterpart to the neutrino IC 191001A. Behaviors of GB6 J2113+1121 are encouraging for the argument that flaring blazars can act as counterparts to IceCube neutrinos (e.g., Halzen & Kheirandish 2016).

It is interesting to compare GB6 J2113+1121 with the 4LAC blazars (Ajello et al. 2020), especially the neutrino-emitting blazar candidates; see Figure 5. GB6 J2113+1121 bears a γ-ray spectral slope typically for 4LAC FSRQs (i.e., 2.44 ± 0.20). The most luminous one among the candidates is PKS 1424-418 while the faintest one is BZB J0955+3551 with a very hard spectrum. TXS 0506+056 is also a very luminous candidate. 1H 0323+342 stands out because of its rather soft spectrum; meanwhile, it is the only radio-loud narrow-line Seyfert I galaxy. The redshift distribution of the candidates is from 0.03 (i.e., 1H 0323+342) to 1.522 (i.e PKS 1424-418). Though the flux level of GB6 J2113+1121 in the quiescent state is low, benefiting from the large variability amplitude, its flux level in the high-flux state is comparable with those of other candidates. Detailed theoretical calculation of neutrino production by GB6 J2113+1121 is beyond the scope of this study, in light of the potential attenuation of the observed γ rays as well as the tangling between the leptonic and hadronic contributions (e.g., Petropoulou et al. 2017; Ansoldi et al. 2018). Future observational evidence, such as orphan γ-ray

[12] IC 191001A is excluded there due to its relatively large angular uncertainty.
[13] https://fermi.gsfc.nasa.gov/ssc/data/access/lat/12yr_catalog/

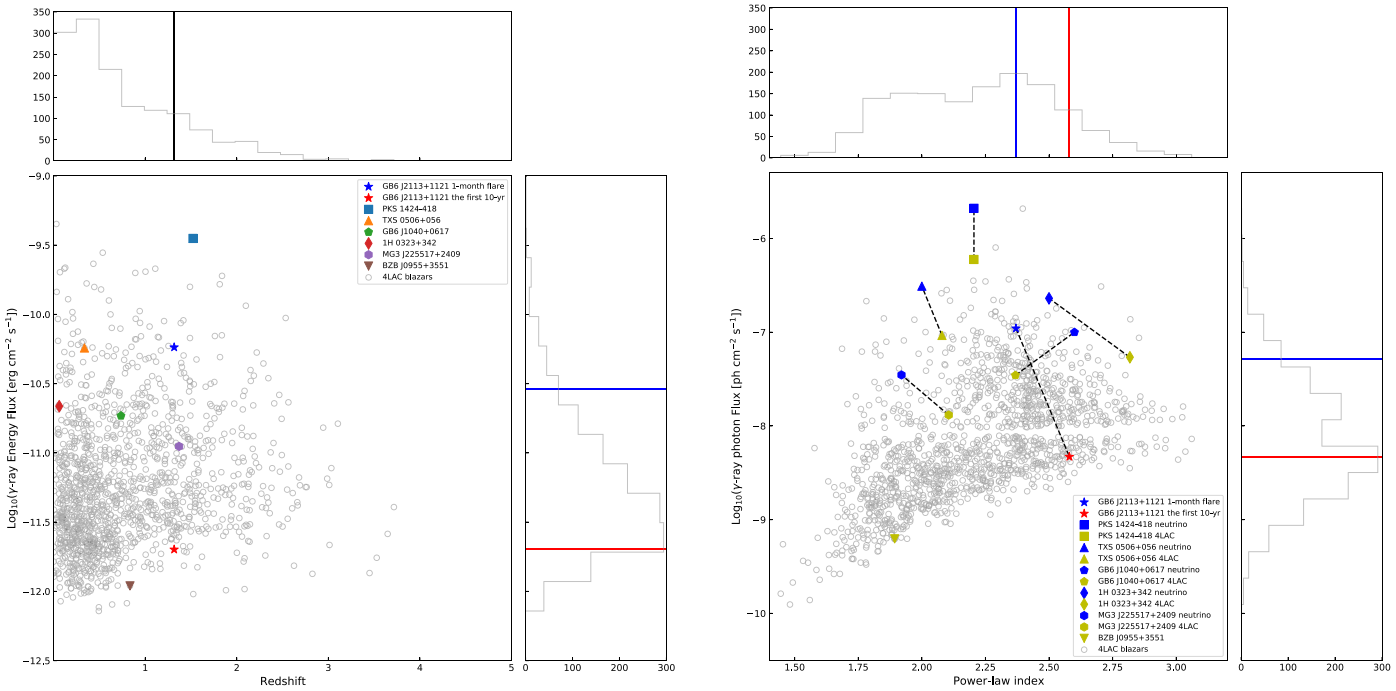

Figure 5. Comparisons between GB6 J2113+1121 and 4LAC blazars (Ajello et al. 2020), in which the known neutrino-emitting blazar candidates are highlighted. The energy ranges corresponding to the energy flux and the photon flux are between 100 MeV and 100 GeV. In the right panel, the 4LAC values of the candidates are colored in yellow; meanwhile, values corresponding to the flares temporally coincident with the arrival of neutrinos (Kadler et al. 2016; IceCube Collaboration et al. 2018a; Garrappa et al. 2019b; Franckowiak et al. 2020) are plotted in blue. For PKS B1424-418, no available spectral information in the high-flux state is found.

flares or X-ray flares that are possibly induced by the secondary particles from the hadronic cascade, are helpful to further investigate the neutrino generation processes.

In summary, the multiwavelength properties of GB6 J2113 +1121 and its potential as a possible neutrino emitter corresponding to IC 191001A are investigated. It is confirmed as the only spatially coincident γ-ray source of the neutrino when it arrives. In 2019 May, a strong γ-ray flare with a flux increase reaching 20 fold and possible spectral hardness then emerged. Violent optical flares in the ZTF *g*, *r*, and *i* bands together with IR ones in the WISE W1 and W2 bands have also been detected. Compared with the detection time of the TDE AT2019dsg, the onset times of the strong γ-ray and optical flares are closer to the arrival time of the neutrino. Meanwhile, the infrared emissions of GB6 J2113+1121 remain in the high-flux state within one month from the arrival time of the neutrino. Benefiting from the temporal information, the by-chance coincidence of GB6 J2113+1121 and IC 191001A is estimated to be $\sim$0.03. Therefore, in addition to the radio-emitting TDE AT2019dsg, the possibility of GB6 J2113+1121 being the counterpart of IC 191001A needs to be considered. Because the blazar is a persistent source, unlike the TDE, from the perspective of the "orphan" neutrino flare of TXS 0506+056 (IceCube Collaboration et al. 2018b), it would be interesting to perform a specific analysis of archival IceCube data to check whether there was a weak neutrino excess in this direction before the TDE. Meanwhile, future detections of more neutrino events toward this direction would be supportive for GB6 J2113+1121 as a neutrino emitter.

This research uses data obtained through the Telescope Access Program (TAP). Observations obtained with the Hale Telescope at the Palomar Observatory were obtained as part of an agreement between the National Astronomical Observatories, the Chinese Academy of Sciences, and the California Institute of Technology. Tapio Pursimo is appreciated for sharing their optical spectrum of GB6 J2113+1121. This research has made use of data obtained from the High Energy Astrophysics Science Archive Research Center (HEASARC), provided by NASA's) Goddard Space Flight Center. This research has made use of the NASA/IPAC InfraredScience Archive, which is operated by the Jet Propulsion Laboratory, California Institute of Technology, under contract with the National Aeronautics and Space Administration. This research makes use of data products from the Wide-field Infrared Survey Explorer, which is a joint project of the University of California, Los Angeles, and the Jet Propulsion Laboratory/ California Institute of Technology, funded by the National Aeronautics and Space Administration. This research also makes use of data products from NEOWISE-R, which is a project of the Jet Propulsion Laboratory/California Institute of Technology, funded by the Planetary Science Division of the National Aeronautics and Space Administration. This study use data based on observations obtained with the Samuel Oschin Telescope 48 inch and the 60 inch Telescope at the Palomar Observatory as part of the Zwicky Transient Facility project. ZTF is supported by the National Science Foundation under grant No. AST-2034437 and a collaboration including Caltech, IPAC, the Weizmann Institute for Science, the Oskar Klein Center at Stockholm University, the University of Maryland, Deutsches Elektronen-Synchrotron and Humboldt University, the TANGO Consortium of Taiwan, the University of Wisconsin at Milwaukee, Trinity College Dublin, Lawrence Livermore National Laboratories, and IN2P3, France. Operations are conducted by COO, IPAC, and UW.

This work was supported in part by the NSFC under grants 11703093, U2031120, 11833007, 12103048, and 12073025, as well as the Fundamental Research Funds for the Central Universities: WK2030000023. This work was also supported

in part by the Special Natural Science Fund of Guizhou University (grant No. 201911A) and the First-class Physics Promotion Programme (2019) of Guizhou University. YLC thank the support from China Postdoctoral Science Foundation Funded Project (BR4260008).

Facilities: Fermi (LAT); Swift; ZTF; Hale (DBSP); WISE.
Software: Astropy (Astropy Collaboration et al. 2018).

ORCID iDs

Neng-Hui Liao https://orcid.org/0000-0001-6614-3344
Zhen-Feng Sheng https://orcid.org/0000-0001-6938-8670
Ning Jiang https://orcid.org/0000-0002-7152-3621
Dong-Lian Xu https://orcid.org/0000-0003-1639-8829
Xin-Wen Shu https://orcid.org/0000-0002-7020-4290
Ting-Gui Wang https://orcid.org/0000-0002-1517-6792

References

Aartsen, M. G., Abraham, K., Ackermann, M., et al. 2017a, ApJ, 835, 151
Aartsen, M. G., Ackermann, M., Adams, J., et al. 2015, ApJ, 807, 46
Aartsen, M. G., Ackermann, M., Adams, J., et al. 2017b, JInst, 12, P03012
Aartsen, M. G., Ackermann, M., Adams, J., et al. 2018, AdSpR, 62, 2902
Aartsen, M. G., Ackermann, M., Adams, J., et al. 2020, PhRvL, 124, 051103
Abdo, A. A., Ackermann, M., Agudo, I., et al. 2010, ApJ, 716, 30
Abdollahi, S., Acero, F., Ackermann, M., et al. 2020, ApJS, 247, 33
Adelman-McCarthy, J. K., Agüeros, M. A., Allam, S. S., et al. 2007, ApJS, 172, 634
Ahlers, M., & Halzen, F. 2015, RPPh, 78, 126901
Ajello, M., Angioni, R., Axelsson, M., et al. 2020, ApJ, 892, 105
Alexander, K. D., Berger, E., Guillochon, J., Zauderer, B. A., & Williams, P. K. G. 2016, ApJL, 819, L25
Alexander, K. D., van Velzen, S., Horesh, A., & Zauderer, B. A. 2020, SSRv, 216, 81
Ansoldi, S., Antonelli, L. A., Arcaro, C., et al. 2018, ApJL, 863, L10
Astropy Collaboration, Price-Whelan, A. M., Sipőcz, B. M., et al. 2018, AJ, 156, 123
Atoyan, A., & Dermer, C. D. 2001, PhRvL, 87, 221102
Becker Tjus, J., Eichmann, B., Halzen, F., Kheirandish, A., & Saba, S. M. 2014, PhRvD, 89, 123005
Bellm, E. C., Kulkarni, S. R., Graham, M. J., et al. 2019, PASP, 131, 018002
Bennett, C. L., Lawrence, C. R., Burke, B. F., Hewitt, J. N., & Mahoney, J. 1986, ApJS, 61, 1
Biteau, J., Prandini, E., Costamante, L., et al. 2020, NatAs, 4, 124
Błażejowski, M., Sikora, M., Moderski, R., & Madejski, G. M. 2000, ApJ, 545, 107
Blandford, R., Meier, D., & Readhead, A. 2019, ARA&A, 57, 467
Blandford, R. D., & Rees, M. J. 1978, in Pittsburgh Conference on BL Lac Objects, ed. A. M. Wolfe (Pittsburgh, PA: Univ. Pittsburgh), 328, http://d-scholarship.pitt.edu/27771/1/PittsburghConference.pdf
Bloom, J. S., Giannios, D., Metzger, B. D., et al. 2011, Sci, 333, 203
Böttcher, M., Reimer, A., Sweeney, K., & Prakash, A. 2013, ApJ, 768, 54
Burrows, D. N., Kennea, J. A., Ghisellini, G., et al. 2011, Natur, 476, 421
Cardelli, J. A., Clayton, G. C., & Mathis, J. S. 1989, ApJ, 345, 245
Cash, W. 1979, ApJ, 228, 939
Condon, J. J., Cotton, W. D., Greisen, E. W., et al. 1998, AJ, 115, 1693
Dermer, C. D., & Schlickeiser, R. 1993, ApJ, 416, 458
Dondi, L., & Ghisellini, G. 1995, MNRAS, 273, 583
Finke, J. D. 2013, ApJ, 763, 134
Franckowiak, A., Garrappa, S., Paliya, V., et al. 2020, ApJ, 893, 162
Garrappa, S., Buson, S. & Fermi-LAT Collaboration 2019a, GCN, 25932, 1
Garrappa, S., Buson, S., Franckowiak, A., et al. 2019b, ApJ, 880, 103
Gehrels, N., Chincarini, G., Giommi, P., et al. 2004, ApJ, 611, 1005
Gezari, S. 2021, ARA&A, 59, 21
Ghisellini, G., Tavecchio, F., Foschini, L., Bonnoli, G., & Tagliaferri, G. 2013, MNRAS, 432, L66
Giommi, P., Padovani, P., Oikonomou, F., et al. 2020, A&A, 640, L4
Graham, M. J., Kulkarni, S. R., Bellm, E. C., et al. 2019, PASP, 131, 078001
Halzen, F., & Kheirandish, A. 2016, ApJ, 831, 12
Healey, S. E., Romani, R. W., Cotter, G., et al. 2008, ApJS, 175, 97
IceCube Collaboration 2013, Sci, 342, 1242856
IceCube Collaboration 2019, GCN, 25913, 1
IceCube Collaboration, Aartsen, M. G., Ackermann, M., et al. 2018a, Sci, 378, eaat1378
IceCube Collaboration, Aartsen, M. G., Ackermann, M., et al. 2018b, Sci, 361, 147
IceCube Collaboration, Abbasi, R., Ackermann, M., et al. 2021, arXiv:2101.09836
Kadler, M., Krauß, F., Mannheim, K., et al. 2016, NatPh, 12, 807
Kara, E., Dai, L., Reynolds, C. S., & Kallman, T. 2018, MNRAS, 474, 3593
King, A., & Pounds, K. 2015, ARA&A, 53, 115
Koay, J. Y., Macquart, J. P., Rickett, B. J., et al. 2011, AJ, 142, 108
Kun, E., Bartos, I., Tjus, J. B., et al. 2021, ApJL, 911, L18
Lei, W.-H., Yuan, Q., Zhang, B., & Wang, D. 2016, ApJ, 816, 20
Levan, A. J., Tanvir, N. R., Cenko, S. B., et al. 2011, Sci, 333, 199
Liodakis, I., Marchili, N., Angelakis, E., et al. 2017, MNRAS, 466, 4625
Liu, H. T., & Bai, J. M. 2006, ApJ, 653, 1089
Loeb, A., & Waxman, E. 2006, JCAP, 2006, 003
Madejski, G. G., & Sikora, M. 2016, ARA&A, 54, 725
Mainzer, A., Bauer, J., Cutri, R. M., et al. 2014, ApJ, 792, 30
Mannheim, K. 1993, A&A, 269, 67
Maraschi, L., Ghisellini, G., & Celotti, A. 1992, ApJL, 397, L5
Masci, F. J., Laher, R. R., Rusholme, B., et al. 2019, PASP, 131, 018003
Mattila, S., Pérez-Torres, M., Efstathiou, A., et al. 2018, Sci, 361, 482
Mattox, J. R., Bertsch, D. L., Chiang, J., et al. 1996, ApJ, 461, 396
Murase, K., Inoue, S., & Nagataki, S. 2008, ApJL, 689, L105
Murase, K., Oikonomou, F., & Petropoulou, M. 2018, ApJ, 865, 124
Murase, K., & Waxman, E. 2016, PhRvD, 94, 103006
Myers, S. T., Jackson, N. J., Browne, I. W. A., et al. 2003, MNRAS, 341, 1
Nolan, P. L., Abdo, A. A., Ackermann, M., et al. 2012, ApJS, 199, 31
Ofek, E. O., Laher, R., Surace, J., et al. 2012, PASP, 124, 854
Padovani, P., & Giommi, P. 1995, ApJ, 444, 567
Padovani, P., Oikonomou, F., Petropoulou, M., Giommi, P., & Resconi, E. 2019, MNRAS, 484, L104
Paliya, V. S., Böttcher, M., Olmo-García, A., et al. 2020, ApJ, 902, 29
Petropoulou, M., Nalewajko, K., Hayashida, M., & Mastichiadis, A. 2017, MNRAS, 467, L16
Planck Collaboration, Ade, P. A. R., Aghanim, N., et al. 2014, A&A, 571, A16
Poutanen, J., & Stern, B. 2010, ApJL, 717, L118
Prochaska, J. X., Hennawi, J. F., Westfall, K. B., et al. 2020, JOSS, 5, 2308
PTF Team 2020, Palomar Transient Factory Level, doi:10.26131/IRSA155, https://catcopy.ipac.caltech.edu/dois/doi.php?id=10.26131/IRSA15
Pursimo, T., Ojha, R., Jauncey, D. L., et al. 2013, ApJ, 767, 14
Rees, M. J. 1988, Natur, 333, 523
Runnoe, J. C., Brotherton, M. S., & Shang, Z. 2012, MNRAS, 422, 478
Scargle, J. D., Norris, J. P., Jackson, B., & Chiang, J. 2013, ApJ, 764, 167
Schlafly, E. F., & Finkbeiner, D. P. 2011, ApJ, 737, 103
Schlegel, D. J., Finkbeiner, D. P., & Davis, M. 1998, ApJ, 500, 525
Shen, Y., Greene, J. E., Strauss, M. A., Richards, G. T., & Schneider, D. P. 2008, ApJ, 680, 169
Sheng, Z., Wang, T., Jiang, N., et al. 2017, ApJL, 846, L7
Sheng, Z., Wang, T., Jiang, N., et al. 2020, ApJ, 889, 46
Sikora, M., Begelman, M. C., & Rees, M. J. 1994, ApJ, 421, 153
Stecker, F. W., Done, C., Salamon, M. H., & Sommers, P. 1991, PhRvL, 66, 2697
Stein, R., Franckowiak, A., Necker, J., et al. 2019, GCN, 25929, 1
Stein, R., Velzen, S. v., Kowalski, M., et al. 2021, NatAs, 5, 510
Tavecchio, F., Ghisellini, G., Bonnoli, G., & Ghirlanda, G. 2010, MNRAS, 405, L94
Ulrich, M.-H., Maraschi, L., & Urry, C. M. 1997, ARA&A, 35, 445
van Velzen, S., Stein, R., Gilfanov, M., et al. 2021, arXiv:2111.09391
Wagner, S. J., & Witzel, A. 1995, ARA&A, 33, 163
Waxman, E. 1995, PhRvL, 75, 386
WISE Team 2019, AllWISE Source Catalog, doi:10.26131/IRSA1, https://catcopy.ipac.caltech.edu/dois/doi.php?id=10.26131/IRSA1
WISE Team 2020, NEOWISE 2-Band Post-Cryo Single Exposure (L1b) SourceTable, doi:10.26131/IRSA124, https://catcopy.ipac.caltech.edu/dois/doi.php?id=10.26131/IRSA124
Wright, E. L., Eisenhardt, P. R. M., Mainzer, A. K., et al. 2010, AJ, 140, 1868
Zauderer, B. A., Berger, E., Soderberg, A. M., et al. 2011, Natur, 476, 425